MODELLING METHODOLOGY AND PRACTICES FOR PERFORMANCE EVALUATION OF AN ELECTRICAL THSA

Haolin MA, Jian FU
School of Mechanical Engineering and Automation, Beihang University
37 Xueyuan Road, Haidian District, Beijing, 100191, China
Phone : +86(0)10 82339022
Email : mhl_buaa@buaa.edu.cn, fujian@buaa.edu.cn

Jean-Charles MARE
Institut Clément Ader (CNRS UMR5312), INSA-Toulouse, Toulouse 31077, France
Phone : +33(0)5 61559717
Email: Jean-charles.mare@insa-toulouse.fr

Tianxiang XIA
Nanjing Engineer Institute of Aircraft System Jincheng, AVIC, Nanjing 211100, China
Phone : +86(0)25 51819900
Email: xiatx@neias.cn

ABSTRACT

With the development of power-by-wire technology, conventional hydraulically powered trimmable horizontal stabilizer actuators (THSA) are being replaced by-all electric types in the latest generation of more electric aircraft (MEA). However, the performance evaluation of an electrical THSA in terms of control dynamics, power sizing, backdrivability, load rejection, thermal management, response to fault, etc. still lacks of well-established preliminary model-based methods and practices. This work deals with the multi-level modelling and simulation of complex multidisciplinary effects, with special considerations to the mechanical transmission of the THSA. Real experiments are used to identify the uncertain model parameters and to validate the proposed models.

KEYWORDS

Electromechanical actuator, incremental modelling, nonlinear effects, parameter identification, trimmable horizontal stabilizer actuator.

I INTRODUCTION

In MEAs, electrohydrostatic actuators (EHA) and electromechanical actuators (EMA) are progressively introduced to replace the conventional hydraulic servoactuators (HSA), which are supplied by a central hydraulic system. While EHAs still use hydraulics internally, EMAs completely eliminate the need for hydraulics and converts electrical energy directly into mechanical energy. However, due to the risk of jamming, EMAs have not yet been widely implemented in primary flight control systems. In latest aircrafts, like the Boeing B787, EMAs are only partially integrated into secondary flight controls such as spoilers, and braking system (Arriola and Thielecke, 2017). The trim horizontal stabilizer (THS) plays a central role in pitch trimming (Figure 1).

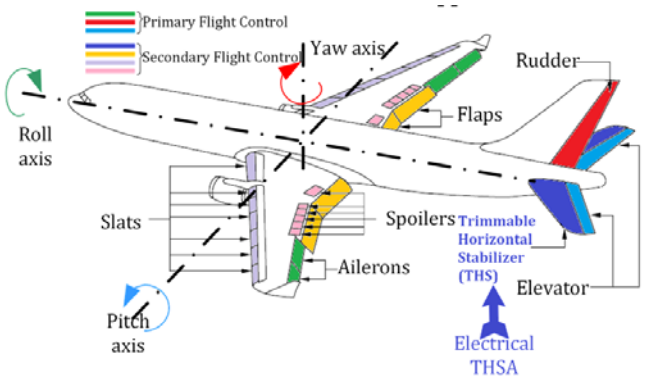

Figure 1. Distribution map of aircraft control surface

Although it is not considered part of the primary flight control surface, the THS surface is substantial, compared with other flight control surfaces. Even small variations in its position can have significant effects on pitch. At present, there is litter literature addressing the incremental virtual prototyping of THSA, with detailed considerations to the mechanical transmission and a system-level view: control dynamics, power sizing, backdrivability, load rejection, thermal management, response to fault, etc. are poorly addressed although they contribute to safety-critical functions.

The proposed communication addresses the model-based engineering of a redundant electrical THSA with special considerations to the mechanical transmission. The application of model-based system engineering (MBSE) methodology is shown to be an effective approach for architecting multi-level models that account for complex multidisciplinary effects and specific engineering requirements. At the functional level, a linear model is provided to facilitate the design of control laws and active/standby path reconfiguration. Hierarchical models are then used to account for nonlinear effects in the mechanical transmission path, including friction, stiffness, backlash, and temperature dependence. In addition, injection of faults is presented to illustrate how models can be used to virtually verify the control algorithms during the development phase of fault-tolerant control systems.

II SYSTEM DESCRIPTION

The architecture of an electrical THSA system is shown in Figure 2. Two electric motors (EM) integrating an independent brake are torque-summed and work in an active/standby mode. They are driven by their respective power drive electronics (PDE) and convert electric power into mechanical power via a gearbox, combining a torque limiter and a speed reducer. The gearbox output shaft drives the screw-shaft of a ball-screw mechanism. The upper and lower claw stops provide the backup mean to limit the ball screw retract and extend runaway movement in case of failure of the software limits.

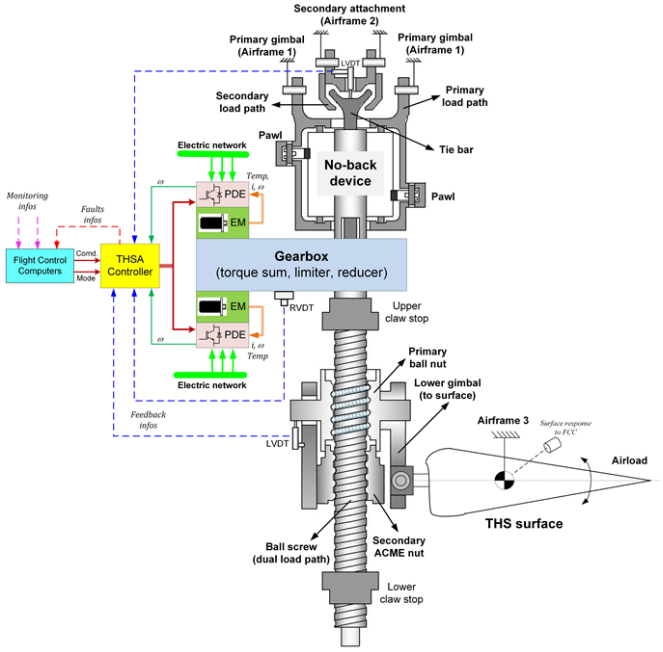

Figure 2. Architecture of the studied electrical THSA

In order to meet the safety requirements, the THSA design makes the THS positioning function fail-freeze. Dual load paths are systematically implemented. The active path is the primary one while the secondary path remains unloaded in normal conditions thanks to a proper backlash with the normal path. Therefore, the secondary path automatically takes over the load transmission in case of failure of the primary path. This concept is implemented for the upper and lower gimbals, and for the nutscrew system. The nut design combines a ball-nut as the primary path and an ACME nut as the secondary one. The screw design resorts on a tie rod located inside the screw as the secondary load path between the airframe and the nut. The fail-freeze response is also ensured by making the THSA irreversible. This is achieved with resort to the motor brakes and the no-back device.

The THSA controller receives commands from, and feeds back, the flight control computers (FCC). The main control structure implements a velocity loop, with an inner EM current loop. The position loop is considered for monitoring purposes. Two Rotational Variable Differential Transformers (RVDTs) measure the screw-shaft angular velocity. Two Linear Variable Differential Transformers (LVDTs) are installed at the upper and lower gimbals to detect the failures of the primary load path or primary ball nut.

III INCREMENTAL MODELLING METHOD

The electrical THSA involves cross-linked physical effects in the electrical, magnetic, mechanical and thermal domains. The models are structured and developed using the Bond-Graph formalism to facilitate the incremental approach, Special attention is paid to the architectures, interfaces and causalities of the models to facilitate their reuse, adaptation, integration and implementation in any other relevant simulation environment. In this way, development time and technical risks are reduced.

Therefore, an incremental modelling approach based on scenario-specific requirements is proposed, as shown in Figure 3, which includes the construction of models with multi-level of complexity and the consideration of various nonlinear and uncertain features. During the model development process, a functional model can be established based on the main function of each component, while a high-fidelity model can be made by integrating various phenomena's, often nonlinear, such as saturation, dead-zone, hysteresis, stiffness, preload, friction, backlash, etc. However, the trade-off between model accuracy and complexity is crucial, as high-precision models require more parameters and complex implementation, and increase the simulation costs.

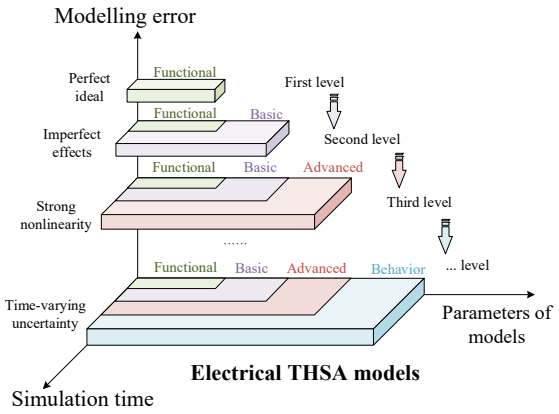

Figure 3. Incremental modelling

3.1 Functional modelling

The THSAs have more complex mechanical load paths than other EMAs. The functional power flow of electrical THSA is presented in Figure 4.

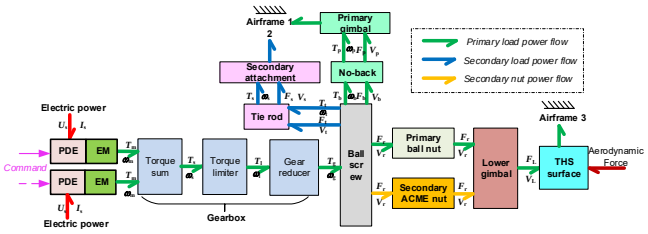

Figure 4. Functional power flow of electrical THSA

Typically, power flows from the electric supply network through the PDE, is converted into mechanical rotational power by the motors and the gearbox assembly, then into

mechanical translational power by the nut-screw, and finally into mechanical rotational power by the 3-bar kinematics to actuate the THS surface.

The functional control loop of the THSA is shown in Figure 5. The model of the controlled system can be numerically linearized for applying the linear control theory for analysis and control design purposes (Fu, Zheng, et al., 2020).

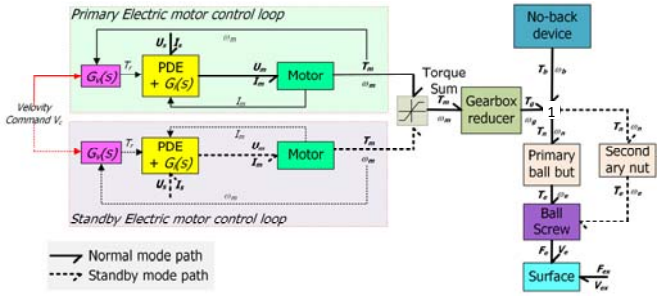

Figure 5. Functional control loop of electrical THSA with power and signal views

3.2 Basic modelling

The PDE and EM can be seen as the electric drive part of electrical THSA. Their models have been previously studied in details (Fu, Maré and Fu, 2017). In the dual-motor electric THSA, the gearbox plays a critical role in the torque-summing of the main and backup EM. The basic model of EM and gearbox is shown in Figure 6. The mechanical compliance of the different elements of the gearbox is considered globally, introducing the overall stiffness (k_g) and equivalent viscous damping (d_g). The inertia of the gearbox is also considered as a single equivalent inertial element (J_g). The basic model of the primary nut-screw can be seen as a series of three linear effects (inertia, friction and compliance), which modelling has already been addressed (Fu, Zheng, et al., 2020).

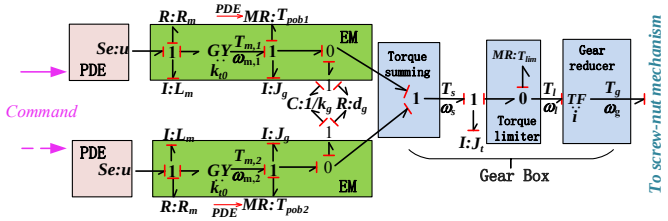

Figure 6. Basic model of EM and gearbox

3.3 Advanced Modelling

The torque limiter, no-back device and dual redundant screw-nuts are quite specific to THSAs. To improve confidence in the high-fidelity model, nonlinear friction and compliance should be paid attention. However, the detailed analysis of the THSA compliance, especially at ball screw, can be found in many previous publications (e.g. Bertolino, Sorli, et al., 2019). Therefore, emphasis is put hereunder on friction effects.

3.3.1 Friction effect in the torque limiter

The torque limiter consists of two friction disks that are pressed against the end face of the large gear using a preloaded disc spring. By adjusting the preload force of the disc spring, it is possible to modify the generated friction torque. The torque limiter and no-back use a similar structure, involving skewed roller friction discs, as shown in Figure 7. In contrast to common carbon disk structure, the disc employs a circular arrangement of inclined rollers.

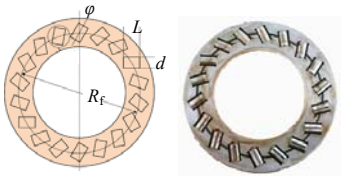

Figure 7. Skewed roller friction disc (SFRD) structure

The torque limiter, Figure 8, enables full torque transmission when it is lower than the maximum static friction torque, thus preventing any slip between the torque limiter shafts. The friction torque has been addressed in a previous study. (Zhang, Fu, Maré et al, 2023).

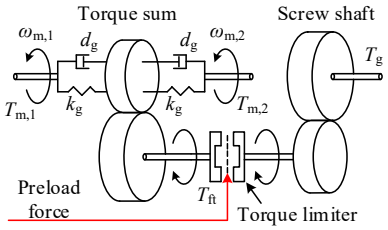

Figure 8. Schematic diagram for modelling the torque limiter

3.3.2 Friction effect of no-back

The function of the no-back device is to prevent the airload to backdrive the THS. The working principle is shown in Figure 9. The friction model has been presented in a previous study (Zhang, Fu, et al., 2023).

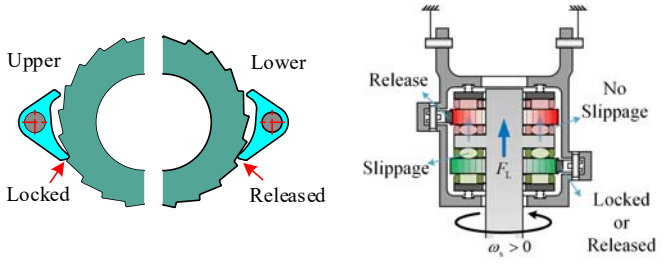

(a) Two-way ratchet pawl (b) Downward movement

Figure 9. No-back device working principal analysis

3.3.3 Friction effect in screw-nuts

In the THSA, the dual redundant screw-nuts consists of a primary ball type nut screw and standby ACME nut screw. The friction F_{fs} between the lead screw and the ball, as well as the friction F_{fn} between the nut and the ball, were modeled using a realistic system-level model (Karam and Maré, 2009). Advanced modelling of the internal friction of the spindle pair requires, first, a comprehensive analysis of the kinematics with multiple degrees of freedom and accurate roll/slide assumptions. Second, the use of the system-level friction model would only slightly affect the simulation realism at the system level, since modelling the no-back device primarily contributes to the THSA irreversibility.

3.4 Behavior modelling

The realization of dual load paths in THSA does not come without technological imperfections. Therefore, the confidence of the simulated response depends highly on the effort placed to make the model realistic when it is intended to virtually assess the different performance indicators.

3.4.1 Redundant load path

The redundancy of the load path of the THSA requires a special attention during the modelling activities. Perfect power transformation and compliance effects are accounted, as shown in the bond-graph model of Figure 10, where the dotted bonds represent the secondary load path. The force and torque are also transported to the no-back and tie-rod models.

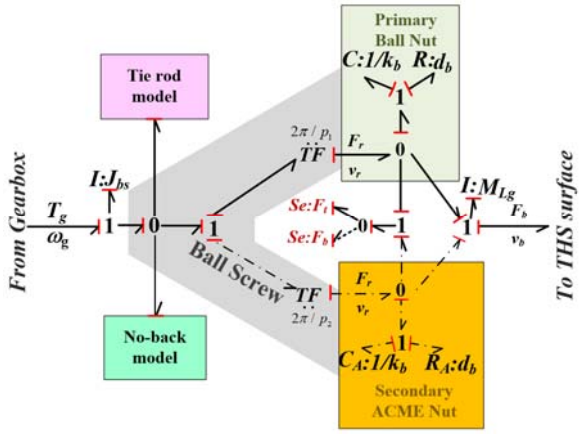

Figure 10. Model of redundant load paths at nutscrew

3.4.2 Temperature sensitivity

Normally, the THSA operates in a temperature range of -55 to 70°C. It has to start-up correctly at low ambient temperature and to not overheat at high temperatures. The internal power losses generate heat and increase the THSA temperatures, especially for the electrical drive part (PDE and EM), which generates a snowball effect by the resulting increase of its power losses. In the mechanical part of the power transmission, temperature has a major effect on friction. First, it increases the lubricant viscosity at low temperature, and therefore the shear force at the loaded dynamic contacts. Second, it makes the solids dilate, which a significant impact on preloads or breakaway forces. In the reported work, a nonlinear parametric function is introduced to modulate the friction force vs. temperature, which identification is addressed in a dedicated section.

3.4.3 Response to faults

As far as it is sufficiently accurate, simulation is a safe and cheap mean to assess the response to a fault. The model version F is dedicated to this purpose by enabling faults to be injected. This point is synthetically addressed in section 5.3.

IV VIRTUAL PROTOTYPING PRACTICE

Due to the complex physical effects, nonlinearities, and uncertainties, it is difficult to develop a pure analytical model including the entire phenomena of the THSA, and a direct experimental test may not be efficient to investigate the effects of each feature. Therefore, a multi-domain simulation platform (Simcenter AMESim in this work) has been used to implement and simulate the models.

4.1 Architecting models with requirements

Complex models increase the simulation times and involve numerous uncertain model parameters. Conversely, models that are too simple may fail to capture the system properties of interest for the current engineering task. Selecting the right model complexity has always been a challenge in implementing virtual prototypes. Therefore, different model levels were developed, as shown in Figure 11.

Model architecting of THSA	Multi-level models							Performance		
	A: Ideal single residual linear model	B: Advanced nonlinear model I	C: Advanced nonlinear model II	D: Advanced nonlinear model III	E: Multiple residual model	F: Fault to fault model	G: Thermal model	Number of parameters	Confidence of parameters	Duration of simulation time
Electric motor										
1. Basic model (resistance, inductance, inertia)	Y							S	H	S
2. Redundancy model (Basic + standby motor model)					Y			M	M	S
3. Advanced model (Basic + iron, friction losses)		Y	Y	Y				L	L	L
4. Fault model (Redundancy model + fault diagnosis)						Y		M	M	L
5. Thermal model (Advanced model + thermal effect)							Y	L	L	L
Mechanical load path										
1. Basic model (efficiency, inertia, linear friction)	Y	Y	Y					S	H	S
2. Redundancy model (Basic + standby load path)					Y			M	M	S
3. Advanced model (Redundancy + real friction, compliance)				Y				L	L	L
4. Fault model (Redundancy model + fault diagnosis)						Y		M	M	L
5. Thermal model (Basic model + thermal effect)							Y	M	L	M
No-back device										
1. Ideal model (linear friction)	Y						Y	S	H	S
2. Basic model (efficiency, inertia/mass, real friction)		Y			Y	Y		M	M	S
3. Advanced model (Basic + real friction, compliance)			Y	Y				L	L	L

Y = Yes; = Not applicable (N/A)

L = Low; M = Medium; H = High

L = Large/Long; S = Small/Short

Figure 11. Matrix of a multi-level approach considering various physical effects.

Depending on what features were considered, two model architectures were developed as shown in Figure 12. Each of these model architectures was built as a supercomponent, and the complexity of each component could be independently adjusted, while meeting the constraints for interfacing with other models. In Figure 12, Model A is the ideal model designed without consideration of system redundancy. It focuses solely on the power transfer relationship between components, with the main effects and their parameters. The Model B considers in addition the motor losses, the inertial and frictional effects of the no-back device. Models C and D are based on Model B, with the addition of compliance characteristics for the no-back device and the primary and standby load paths. Model E fully models the THSA system with a guaranteed low model wizard. Model F enables faults to be injected. Finally, Model G introduces a temperature sensitivity to Model A and links it to each set of lumped parameters via a functional relationship.

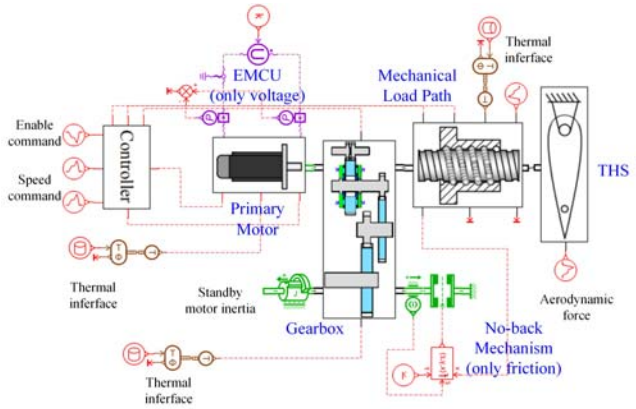

(a) Single residual system model architecture (Model G)

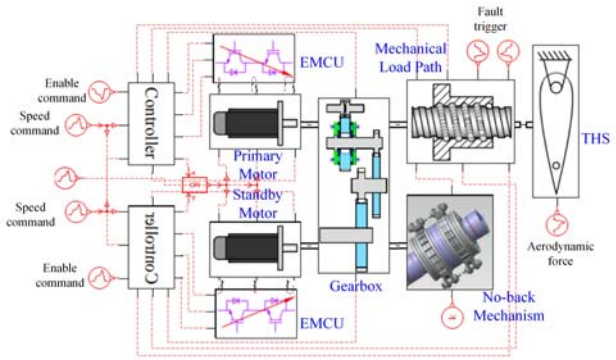

(b) Multiple residual system model architecture (Model F)

Figure 12. Example of implementation models

4.2 Identification of uncertain parameters

In low temperature environment, some parameters may drift with temperature. Although this process is usually slow, the accuracy of the model can degrade significantly with large temperature changes from the reference temperature.

Hence, system parameter identification methods are used to estimate parameters at typical temperature points based on the esperimental data obtained at very low temperature, as shown in Figure 13. The differential evolution (DE) algorithm, a heuristic algorithm based on differential mutation and real-coded, was used for parameter identification (Ma, Fu and Xia, 2023). According to the algorithm and procedure described above, the data obtained with the experimental devices are presented in the following section.

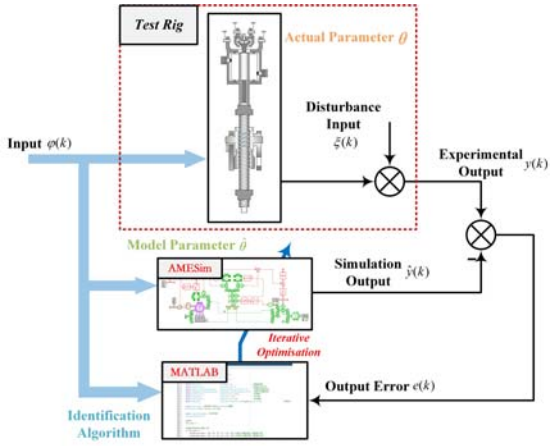

Figure 13. Process of model parameter identification

4.2.1 Identification of the friction coefficient of no-back device

The friction of the no-back device depends on the friction torque generated at the friction disc. To study the variation law of the friction torque, a friction disc performance test rig was designed and is shown in Figure 14. Figure 15 compares the identified friction torque with the experimental results, indicating a good fit and high confidence in the results.

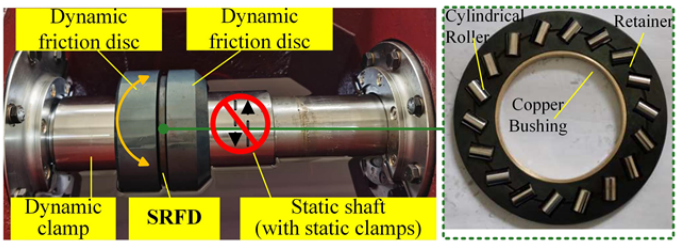

Figure 14. The test rig for friction disc in torque limiter and no-back device

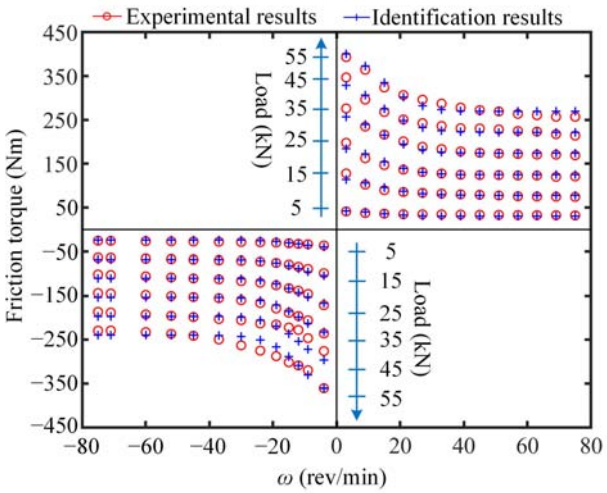

Figure 15. The friction of no-back identification results

4.2.2 Identification of the stiffness coefficient

The parameters to be identified are the structural stiffness and damping coefficients at nutscrew. The test data were obtained using the electrical THSA testbench. The displacement of the rudder surface when the actuator stops actuating can be approximately considered as the load path deformation caused by the load force. The particle DE optimization algorithm was used and provided a good fitting and confidence, as shown by the parameter identification and load force fitting results.

4.2.3 Identification of temperature sensitivity

Eight sets of data were collected for operation at temperatures 5°C, 0°C, -10°C, -20°C, -30°C, -40°C, -50°C, and -55°C, for 8 operating speeds. The relationship between the friction torque of the gearbox, the temperature, and velocity is shown in Figure 16. Logically, the friction torque increases at low temperatures and low speeds. The same measurements and plots were also made for the nut-screw.

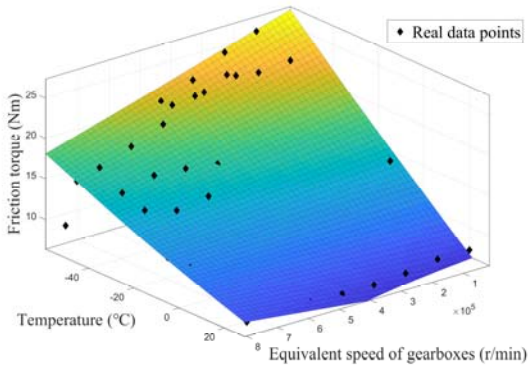

Figure 16. Friction versus temperature and speed - Fitted surface plots for gearbox

V RESULTS AND DISCUSSION

The experimental platform used to identify and validate the model is shown in Figure 17. An industrial EMA is used as a dynamic loading device, and a heavy disk at one end of the lever reproduces the inertia of the THS. The test rig can be used to measure or identify backdrivability, friction, compliance/backlash, sensitivity to low temperature operation, and to assess the THSA response to faults.

5.1 Backdrivability

The THSA backdrivability depends primarily on the friction torque of the no-back device. To test it, a four-period velocity command with a positive ramp aerodynamic compressive force was applied at time 1 s. Bipolar trapezoidal trim velocity commands with an amplitude of 15 mm/s and acceleration of 30 mm/s² were applied at times 1 s and 6 s, respectively.

Given the compressive air load, the lower pawl disc locks when the THS is aiding, while the upper pawl disc remains released, as shown in Figure 18(a). The simulation results of Model B in Figure 18(b) show that the change in the operating condition of the pawl affects the no-back friction torque between opposing and aiding load conditions. Model A does not reproduce this real behavior. There is a difference in the motor current (Figure 18(c)), which probably comes from the friction model parameters.

The speed tracking curve of the motor in the experiment, as depicted in Figure 18(d) for Model C, exhibits distortion at time 6 s, due to the presence of the no-back device which operated under an aiding load. This phenomenon arises when the load surpasses the preload, resulting in a sudden increase in the friction torque.

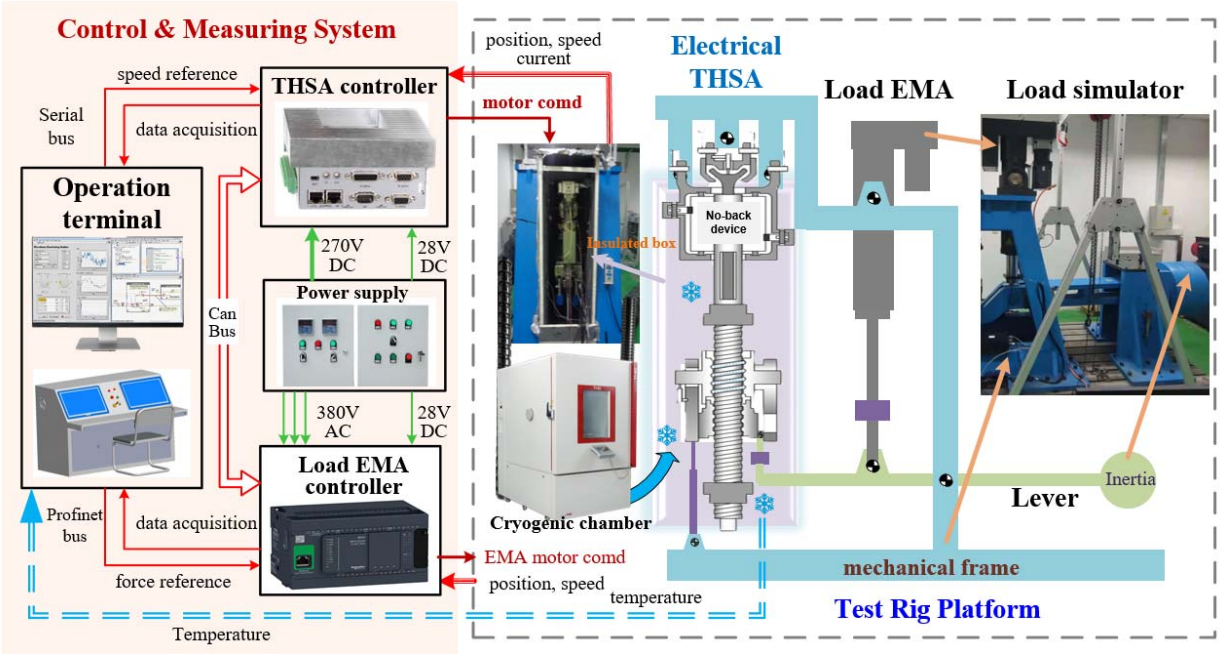

Figure 17. Structure of electrical THSA performance test rig

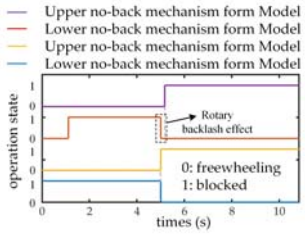

(a) Ratchet pawl mechanism in operation

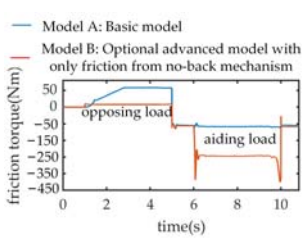

(b) No-back device friction torque

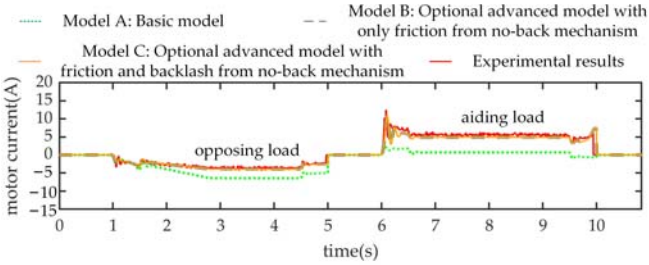

(c) The current response in motor operation

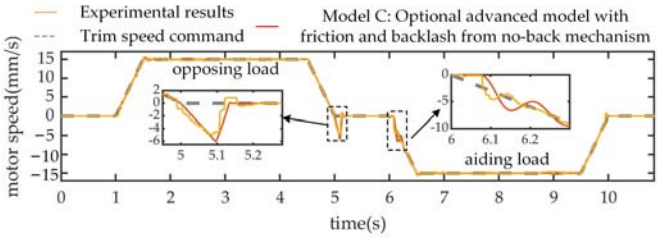

(d) The speed response of model C and test

Figure 18. Simulated and experimental responses showing the nonlinear effects

5.2 Low temperature sensitivity analysis

Low temperature tests were conducted on the test rig to analyze the sensitivity of the THSA performance to temperature. The electrical THSA was enclosed in an insulated box, with only air inlet and air outlet connected to the cryogenic chamber. A velocity ramp of 9 mm/s was applied, while the loading actuator maintained a constant force of 55 kN. In the insulated box, the temperature was set to -30°C. Due to the influence of temperature on the THSA behavior, a single control law set for 25°C operation may not be appropriate at -30°C. Therefore, an optimization method was applied to set the control law, as reported in a previous work (Ma, Fu and Xia, 2023).

Figure 19 illustrates the velocity and current responses when the flight surface was subjected to a velocity ramp of 9 mm/s with an acceleration of 30 mm/s^2, while the loading actuator maintained a constant force of 55 kN.

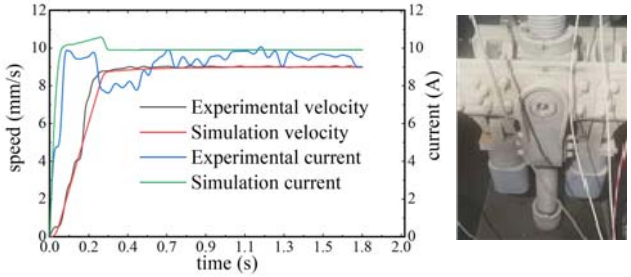

Figure 19. Performance of THSA under low temperature

The functional model of electrical THSA demonstrated high accuracy, as indicated by an average speed error of only 0.58%.

5.3 Response to faults

A reasonable fault modelling and simulation can help reduce the cost and risk of fault injection during experiments. This approach enabled the simulation responses with experimental data, focusing on mechanical fault modes such as jamming fault, primary load path fault, and electric motor faults.

5.3.1 Jamming fault

The jamming faults were introduced into the simulation model by mechanically locking the surface at time 3.5 s. For test verification, the jamming faults were injected by adjusting the position of the limiting bolts on the test rig. Once the jamming faults occur, the motor torque increases rapidly to overcome the large load force caused by the surface jamming (as shown in Figure 20(a)) and eventually exceeds the maximum static friction torque of the torque limiter. This makes its input and output shafts slip (Figure 20(b)), causing unsynchronized velocity feedback from the RVDT and the motor position sensor (Figure 20(c)).

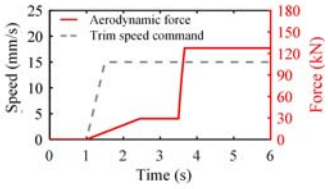

(a) Trim speed command and aerodynamic force input

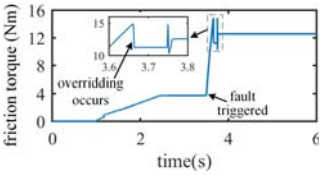

(b) Friction torque generated from torque limiter

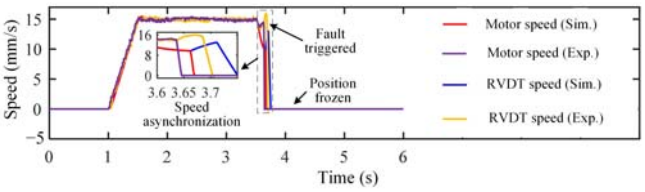

(c) Trim speed feedbacks from different sensors

Figure 20. Simulation and experimental response to jamming

5.3.2 Primary load path fault

A load path failure was simulated by inserting a gap between the upper gimbal and the fuselage at time 7.5 s. Failure was also artificially injected during experimental study by disconnecting the upper gimbal from the frame of the test rig. Figure 21 shows the simulation and experimental responses in the case of primary load path failure. The velocity commands and loading forces are plotted in Figure 21(a). The changes in load force in the primary and standby load paths, as well as the changes in the assembly gap in the standby load path (Figure 21(b) and Figure 21(d)), show that the standby load path remains unloaded in normal operation due to the initial assembly gap. As part of the fault isolation and reconfiguration process, both primary and backup motors are shut down. At this point, the actuator enters into a locked fault-tolerant mode and loses its normal actuation function (Figure 21(c)).

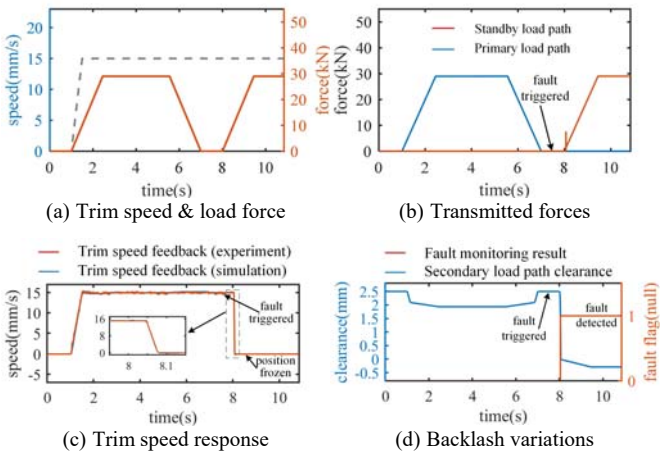

(a) Trim speed & load force (b) Transmitted forces

(c) Trim speed response (d) Backlash variations

Figure 21. Response to primary load path fault

5.3.3 Response to motor fault

During the experiment test, a reverse command with an amplitude of 5 mm/s and an acceleration of 20 mm/s^2 is first sent to the THSA, while the load force is set to a constant tensile load of 20 kN, which acts as an aiding load. An electrical fault is injected by disabling the primary motor at time 1.8 s then activating the electrical standby channel 15 ms later. This delay is representative of the time required to identify the fault, reconfigure, and engage the electrical standby channel.

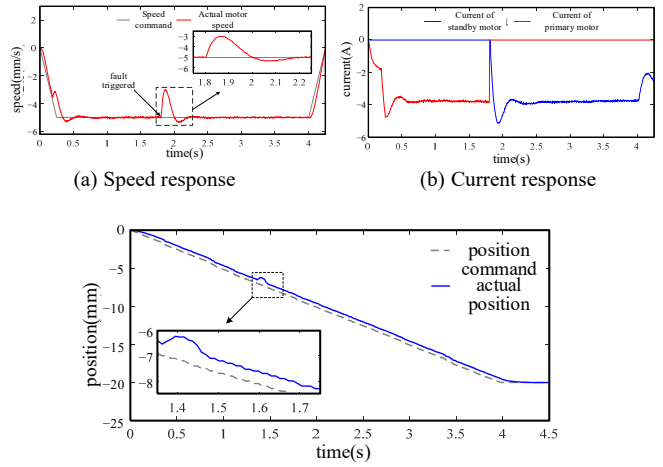

(a) Speed response (b) Current response

(c) Position tracking

Figure 22. Switching performance between two channels

Figure 22(a) and (b) show the motor speed tracking and current tracking performance curves. A reverse position command with a position amplitude of 20 mm and a velocity amplitude of 5 mm/s is sent. At time 1.35 s, an electrical fault is injected by disabling the primary motor and applying a tensile airload force of 20 kN plus 40 kN/s. The electrical backup channel in engaged 15 ms later. The measured position tracking of the electrical THSA is shown in Figure 22(c). Figure 22 (a) and (c) also show that the speed and position tracking performance gradually recover once the standby motor is activated, indicating that the THSA maintains its normal actuating function. However, during channel switching, nonlinear stiffness and anti-reversion friction may have adverse effects, resulting in an adjustment time of about 0.15 s required for the velocity and position tracking to match normal operating conditions.

CONCLUSION

This paper has proposed a model-based and simulation-aided performance evaluation methodology for an electrical THSA. This approach also helps gaining practical experience for the application of EMA, and facilitates the subsequent implementation of EMA on primary flight control surfaces. The main contributions are firstly the detailed study of the operating principle and nonlinear effects of key components of electrical THSA, including the gearbox, mechanical load path, and no-back device. Secondly, based on the incremental modelling approach, a multi-level nonlinear model has been established given the requirements to verify and the different operating scenarios. Special attention has been paid to the trade-off between model complexity and realism, and to the identification of the uncertain model parameters. Last, in accordance with the functional requirements of the electrical THSA, a test methodology was used to assess the electric THSA prototype. It involved a comprehensive excitation, measurement and control approach to facilitate the performance evaluation.

REFERENCES

Arriola D and Thielecke F. (2017), *Model-based design and experimental verification of a monitoring concept for an active-active electromechanical aileron Actuation System*, Mechanical Systems and Signal Processing; 2017; 94:322–45.

Bertolino AC, Sorli M, et al. (2019), *Lumped parameters modelling of the EMAs' ball screw drive with special consideration to ball/grooves interactions to support model-based health Monitoring*, Mechanism and Machine Theory; 2019; 137:188–210.

Fu J, Maré J-C and Fu Y. (2017), *Modelling and simulation of flight control electromechanical actuators with special focus on model architecting, multidisciplinary effects and power flows*, Chinese Journal of Aeronautics 2017; 30(1):47–65.

Fu J, Zheng C, Maré J-C, et al. (2020), *virtual prototyping of electrical THSA focused on mechanical power transmission functions*, 32nd Congress of the International Council of the Aeronautical Sciences, ICAS 2020.

Karam W and Maré J-C. (2009), *Modelling and simulation of mechanical transmission in roller-screw electro-mechanical actuators*, Aircraft Engineering and Aerospace Technology; 2009; 81(4):288–98.

Ma H, Fu J and Xia T. (2023), *Optimization Methods for the Control Law of an Electrical Trimmable Horizontal Stabilizer Actuator Operating at Low Temperatures*, 2023 9th International Conference on Control, Decision and Information Technologies. IEEE, 2023.

Zhang W, Fu J Maré J-C, et al. (2023), *Investigations on MBSE modelling and dynamic performance assessment of an electrical trimmable horizontal stabilizer actuator*. Chinese Journal of Aeronautics 2023.